

# Analyzing the Sheet Metal Extrusion Process Using Finite Element Analysis

Amit Bhumarker<sup>1,\*</sup>, Abhishek Singh<sup>2</sup>

## Abstract

A wide range of sheet metal forming techniques has been developed to make it easier to produce intricate 3D objects. However, the knowledge still isn't sufficient. The sheet metal extrusion method was examined in this research as one of the common sheet-bulk metal manufacturing technologies. Consideration of the flow-stress curve's impact across a broad range of plastic strain and ductile damage played a pivotal role in constructing a realistic finite element method (FEM) model for the sheet metal extrusion process. The model was subsequently simulated using an Arbitrary Lagrangian-Eulerian (ALE) FEM, implemented in MSC. Marc. Validation of various phenomenological characteristics, such as metal flow behavior, shrinkage cavity, and the effects of different combinations of punch, extrusion outlet, and pre-punched hole diameter, was achieved by comparing the results with experimental data. These findings serve as a theoretical basis for the design of sheet metal extrusion processes.

**Keywords:** Sheet Metal, Finite Element Method, Arbitrary Lagrangian-Eulerian, Metal Flow Behavior, Shrinkage Cavity.

## INTRODUCTION

The automotive industry's demands for robust, high-performance, and accurately finished functional 3D components have led to a current boom in the development of the sheet-bulk metal forming technique, which makes it easier to produce these intricate 3D parts [1]. To make components with a protruded portion or a blind cavity as the positioning element, stamping or ne-blanking is frequently coupled with sheet metal extrusion, one of the most common sheet-bulk metal forming methods. Punch penetration and extrusion occur simultaneously throughout the sheet metal extrusion process, and significant deformation occurs during the procedure. As a result, the deformation mechanism cannot be studied using the standard analytical technique, and there is still a lack of knowledge regarding this process. The process design frequently relies on time-consuming trial-and-error testing.

It is now feasible to thoroughly analyze the sheet metal extrusion process because of the rapid development of the finite element technique (FEM). Using proprietary rigid-plastic FEM software [2] analysis of such a process that improved and assumed strain FEM and the arbitrary Lagrangian-Eulerian (ALE) FEM, respectively, were used to simulate the sheet metal extrusion process [3, 4, 5].

These published documents, however, mostly concentrated on the simulation approach itself. The suggested approach was only tested using the sheet metal extrusion procedure. As a consequence, a numerical model of the sheet metal extrusion

### \*Author for Correspondence

Amit Bhumarker  
E-mail: amitbhumarker2@gmail.com

<sup>1,2</sup>Assistant Professor, Department of Mechanical Engineering, Annie Institute of Technology & Research Centre, Chhindwara, Madhya Pradesh, India

Received Date: December 17, 2023  
Accepted Date: January 08, 2024  
Published Date: February 08, 2024

**Citation:** Amit Bhumarker, Abhishek Singh. Analyzing the Sheet Metal Extrusion Process Using Finite Element Analysis. International Journal of Fracture Mechanics and Damage Science. 2023; 1(1): 13–25p.

process was created in this work and verified using the same experimental conditions. Research on the metal flow behavior, stress/strain distribution, and progression of ductile damage in the sheet metal extrusion process were researched and described based on this verified model.

There were five sections in the entire document. First, in Section 2, a numerical sheet metal extrusion model was provided along with a material model of choice and ductile fracture criteria. Additionally, the method for calculating the critical damage value was implemented. In Section 3, the relevant experimental tool design and data-gathering system were covered. The numerical model of the sheet metal extrusion process was then validated by comparing simulation and experiment. Based on this model, Section 4 examined the metal behavior, stress and strain distributions, the evolution of ductile damage, and effects of various combinations of punch, die, and pre-punched hole diameters on the forming force. In Section 5, several findings were provided.

## NUMERICAL MODEL

### Sheet Metal Extrusion

The sheet metal is securely gripped between the guide plate and the die at the start of the sheet metal extrusion process. The sheet metal is then penetrated by the punch and extruded in the direction of the die's extrusion exit. Before the sheet metal extrusion process, a hole may occasionally be pre-punched, allowing the material to flow without significant restriction in the radial direction and reducing the amount of forming force needed.

A numerical model was suggested from the perspective of the mentioned occurring, as seen in Figure 1. In Table 1, a range of boundary conditions and geometrical features for the sheet metal extrusion process are provided. The tools were modeled as rigid bodies, and the friction was represented using the Coulomb friction law. After that, simulations were run using an ALE FEM that was integrated into MSC. Marc. This method's comprehensive information is included in a prior study [5], which is available.

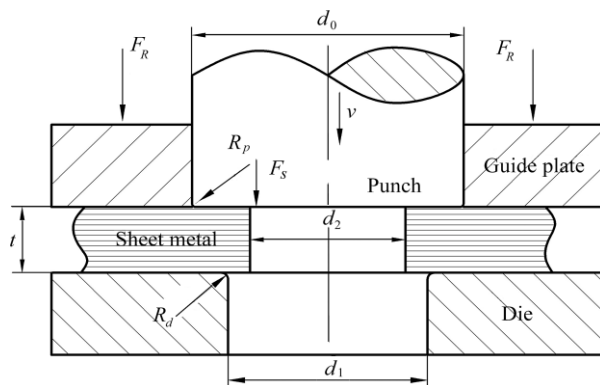


**Figure 1:** Numerical Model

**Table 1.** Process parameters

Process parameters	Values R
Radius of punch edge ( $R_p$ ) (mm)	0.2
Diameter of punch ( $d_0$ ) (mm)	11
Diameter of extrusion outlet ( $d_1$ ) (mm)	0, 5, 6, 8, 10
Diameter of pre-punched hole ( $d_2$ ) (mm)	0, 4, 6, 8
Sheet metal thickness ( $t$ ) (mm)	5
Blank Holder Force ( $F_r$ ) (KN)	60
Velocity of punch ( $v$ ) (mm/s)	10
Friction coefficient ( $\mu$ )	0.1

## Material Model

To extrapolate the yield stress curve based on the results of standard tensile tests, material models such as Voce, Ludwik, Swift, Gosh, the Hockett-Sherby model (H-S model) [6], and the modified H-S model [7] are frequently required. This is because the real plastic strain obtained from tensile tests is very small, while the sheet-bulk metal forming process produces localized severe deformation with a large strain.

However, the applicability of these models should be assessed before integration into the FEM programme. A validation scheme for various material models based on tensile and torsion tests using C45E steel was presented since a greater plastic strain range may be obtained based on torsion tests. The flow stress curves from these two experiments are shown in Figure 2, together with several additional curves (curves 2, 3, 4, 7, and 8) that were extrapolated based on the results of tensile tests with various material models. The result generated from the modified H-S model (curve 5) is somewhat more coincident with the torsion test result (curve 6) when the extrapolation results are compared to the torsion test result. As a result, the modified H-S model was utilized to generate the large strain range flow stress curve. 100% spheroidized C15E steel with a 5 mm thickness was used as the study's material. The final flow stress curve was characterized using the modified H-S model as

$$K_f = 541 - (541 - 233) \exp(-3\varepsilon_p^{0.71}) \quad (1)$$

Where,  $K_f$  represents the flow stress, and  $\varepsilon_p$  represents plastic strain. Due to the low velocity of the punch, the effect of the variance of the strain rate on flow stress is not taken into account [1].

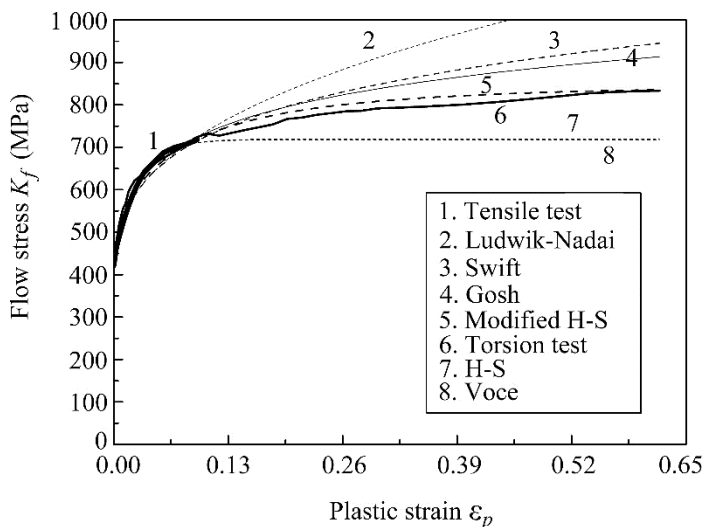


**Figure 2.** Comparison between extrapolation and experiment results.

## Ductile Fracture Criterion

Whether the necessary deformation can be achieved without the material failing is a key issue in metal forming. When a metal is subjected to significant strain, voids start to develop, grow, and merge, resulting in ductile damage. Carrying out a standard finite element simulation and post-processing the finite elements using ductile fracture criteria to find zones where fracture hazards might develop are two ways to represent the aforementioned damage. A variable most frequently referred to as damage can be used to reflect the state of the material before it fractures. The fundamental tenet of the majority of ductile fracture criteria is that the material is considered to have failed when the damage exceeds a critical value [8].

The inclusion spacing-to-size ratio is connected to this essential number. Analytical research on the development of spherical voids in a completely plastic matrix was conducted by Rice and Tracy [9]. Failure was predicted to happen whenever the cavity radius reached a certain amount. The stress and

strain histories of the material have a significant influence on the growth and coalescence of voids. Consequently, the deformation history is needed when modeling fracture initiation. The aforementioned histories are often included as part of the local ductile fracture criterion. In general, they can be defined as an integral of the actual stress state over the corresponding plastic strain up to the fracture.

A modified version of the Rice and Tracy criterion [10], which was developed specifically for the damage evolution of sheet-bulk metal forming, was applied in this work as follows:

$$\int_0^{\epsilon_f} \exp(1.5 \frac{\sigma_m}{\bar{\sigma}}) (1 + C_1 \left| \frac{\sigma_3'}{\sigma_1'} \right|) d\epsilon^p = C \quad (2)$$

Where  $C_1 = 0.5$  and  $C = 1.82$  for 100% spheroidized C15E steel, respectively.

### EXPERIMENTAL PROCEDURE

The forming force from the simulation and that from the experiment were compared to ensure that the simulation had been validated. An internal data collection system [11] was created to measure the force-stroke curve, and Figure 3 depicts the experimental tool design for the sheet metal extrusion process. The data collection system is based on the electrical measuring method. The punch is fitted with complete bridge positioning strain gauges to measure force, and a displacement transducer is utilized to gather the corresponding stroke data concurrently. On a device for evaluating materials, the strain gauges were calibrated. Figure 4 depicts the basic idea behind the electrical measurement technique.

A 3200 KN double-action hydraulic press with separately adjustable blank holding force and ejector force was used for the experiment.

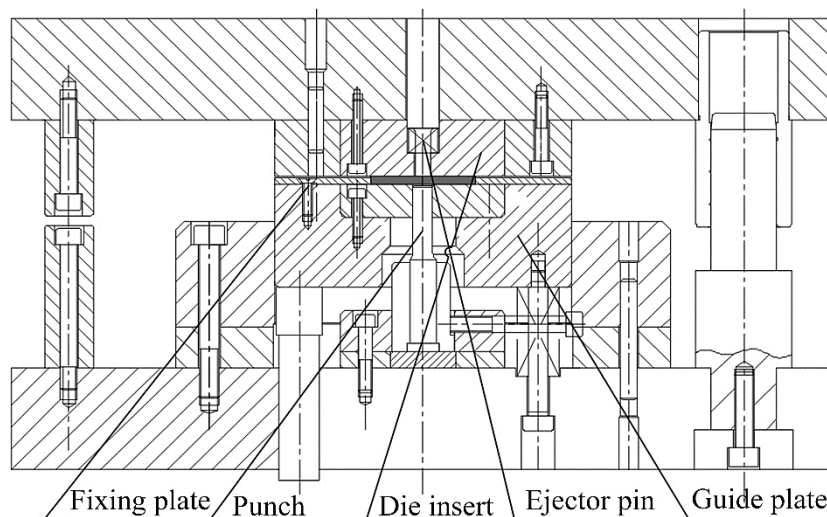


**Figure 3.** Experimental tool design.

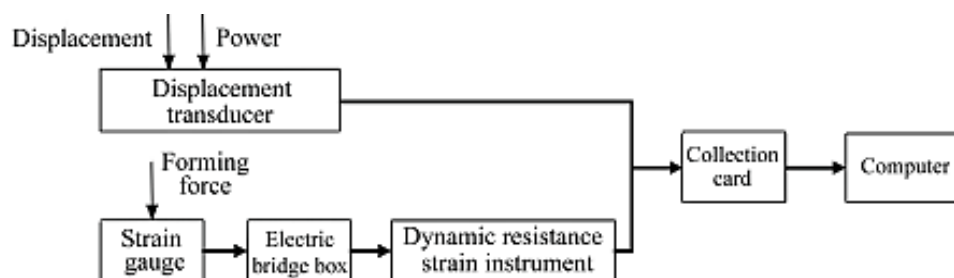


**Figure 4.** Principle of the electrical measuring method.

The distribution of equivalent plastic strain in the deformation zone was calculated using the coordinate grid technique (CGM) in addition to the force-stroke curve [12]. The initial carved coordinate grid on the meridian surface is seen in Figure 5. The distribution of plastic strain on the final grid after deformation may be estimated using a large strain analysis approach to compare with the simulation findings.

## RESULTS AND DISCUSSION

The comparison of the force-stroke curve between an experiment and a simulation is shown in Figure 6 a, b. The findings were comparable, and the estimated error was around 10%. The assumption of a stiff tool caused a little difference in the growing tendency just at the beginning of the force-stroke curve. The geometrical characteristics of the deformed portion and the simulation's findings show a strong correlation.

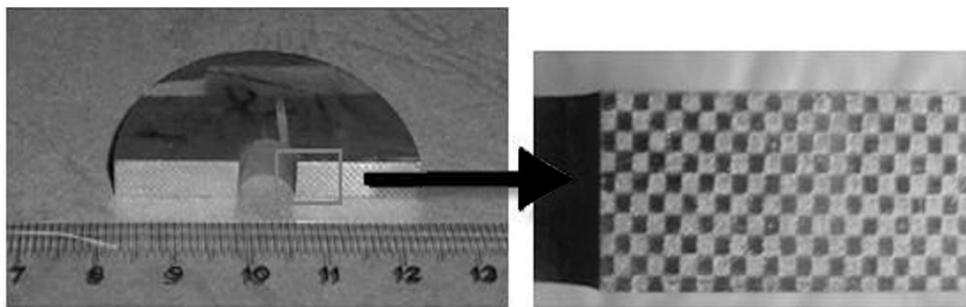
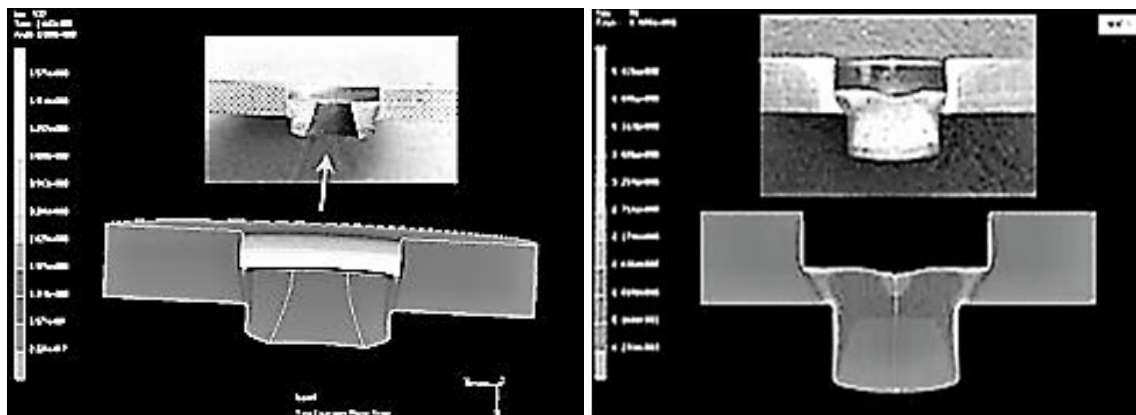
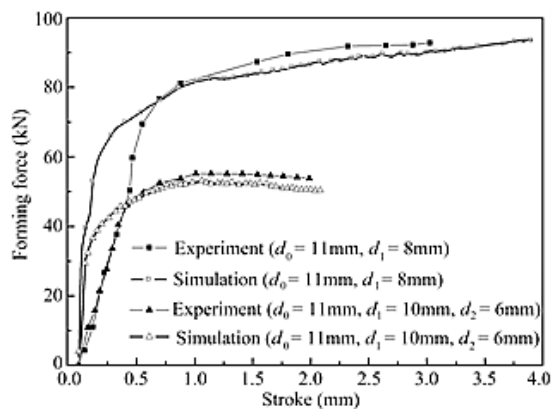


Figure 5: Initial etched coordinate grid on the meridian surface



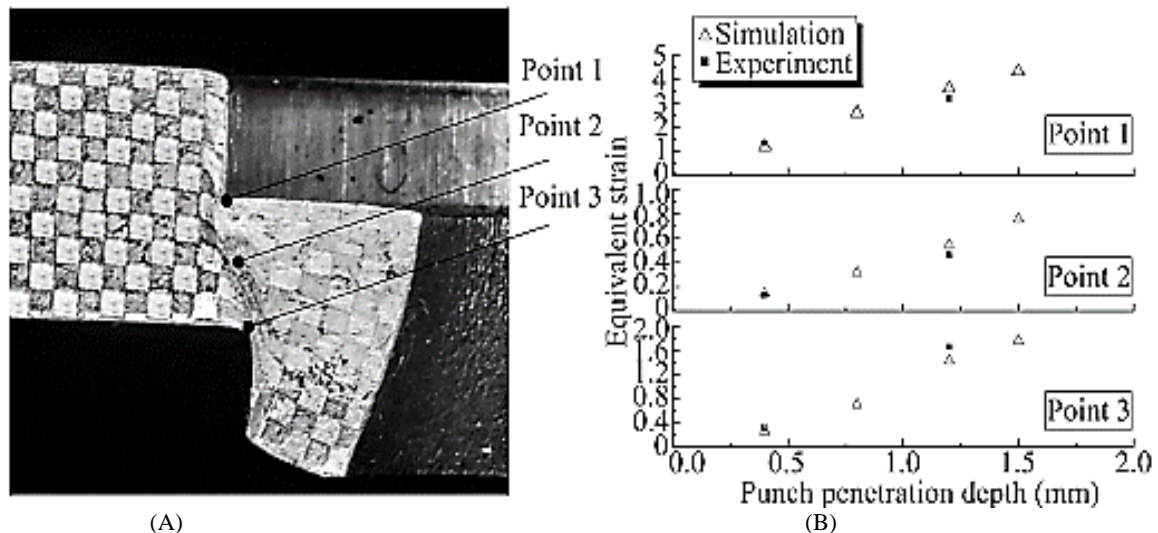
(A)



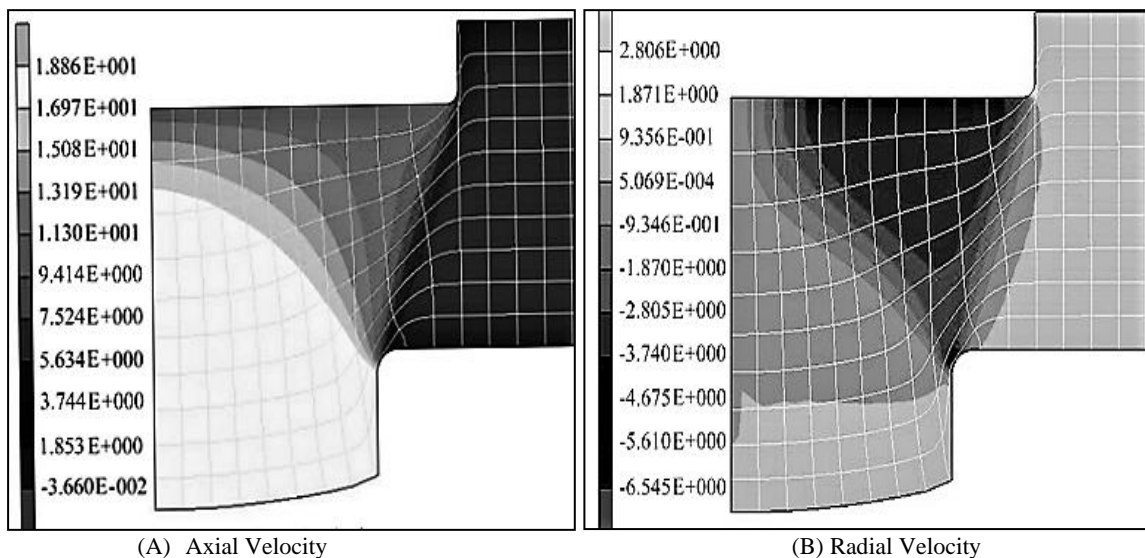
(B)

Figure 6. Comparison between experiment and simulation data. (a) Geometrical results; (b) Force-stroke curves

Additionally, Figure 7 a,b displays the equivalent plastic strain values calculated for the final grid after deformation at three points under various punch penetration depths. Only 15% separated these two results.



**Figure 7.** Comparison of the distribution of equivalent plastic strain. (a) Specimen after deformation; (b) Distribution of equivalent plastic strain.



**Figure 8.** Shows the velocity field distributions for a 25% punch penetration (C15E,  $t = 5$  mm).

### METAL FLOW BEHAVIOR

When a punch penetrates a piece of material by 25%, Figure 8 a,b displays the velocity field distribution in the deformation zone. As illustrated in Figure 9, the deformation zone may be split into three distinct domains based on the interaction of axial and radial velocities: the deformed, deforming, and rigid domains. The direct division of the deformation zone is shown in the picture. The material has finished deforming in the deformed domain and is now firmly moving towards the extrusion exit. While there was no deformation in the rigid domain, there was significant deformation in the deforming domain. Material was stretched, compressed, and rotated in this field accordingly. It eventually entered the extrusion outlet. The division method of the deformation zone discussed above is also practical for the sheet metal extrusion process with various beginning sheet metal thicknesses, as illustrated in Figure 10 a,b,c.



The residual thickness of the sheet metal between the punch and die reduced as punch penetration increased, along with the difference in axial velocity between the centre and surrounding components. As a result, it was difficult for the material to flow around the die edge to make up for the deficiency of material close to the axis. The lack of material around the axis would also be influenced by the friction force between the material and the die, the subsidiary tensile stress caused by the extrusion punch penetration into the material, and the limitations of the guide plate. As can be seen in Figure 11, the shrinkage cavity developed as a result of the punch penetrating the material by a factor of 55 per cent.

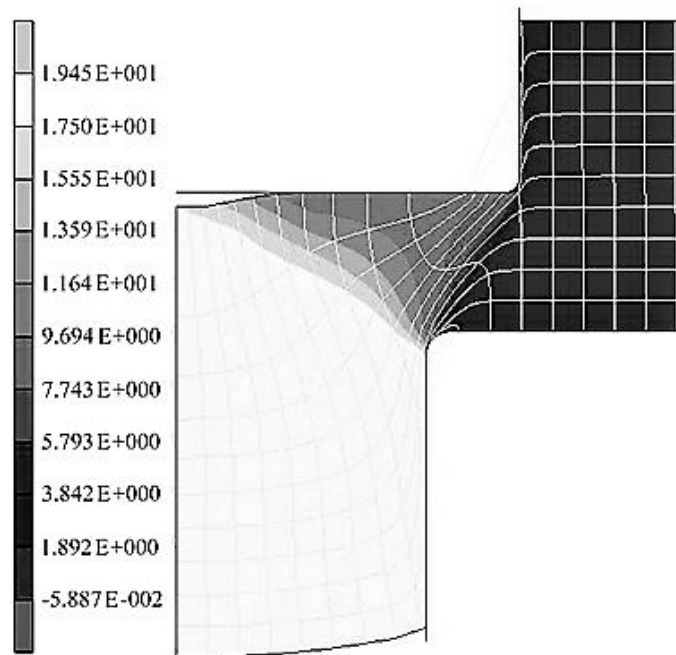


**Figure 11.** Phenomenon of shrinkage cavity (C15E,  $t = 5$  mm).

In Figure 12, the relationship between the frequency of shrinkage and the radius of the punch edge ( $R_p$ ) and die edge ( $R_d$ ) is shown. It is clear that shrinkage was more common when  $R_d$  was smaller, but this occurrence decreased as  $R_p$  increased.

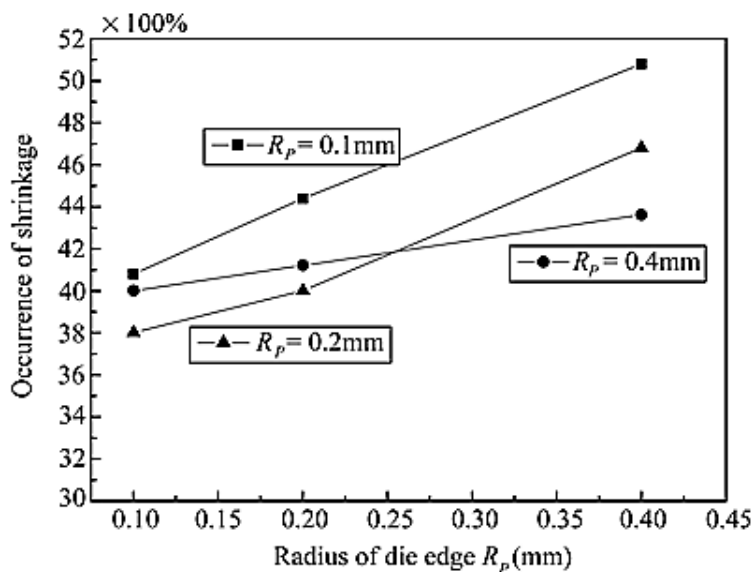


**Figure 12.** Effect of  $R_p$  and  $R_d$  on the occurrence of shrinkage cavity.

A pre-punched hole somewhat lessened the radial and axial flow restrictions, and various combinations of the pre-punched hole and extrusion outlet had distinct effects on the limitation in the two directions. The velocity field distributions when  $d_2 \approx d_1$  were, as shown in Figures 13(a) and (c), relatively comparable to the ones in Figure 8 but with a larger material revolution. For the situation where  $d_2 > d_1$ , the velocity field distributions were displayed as in Figure 13(b) and (d), which resembled a ring-upsetting process. The velocity distribution was converted to  $d_2 < d_1$  up to the dynamic shear zone, which coincided with the line, punch, and die edges.

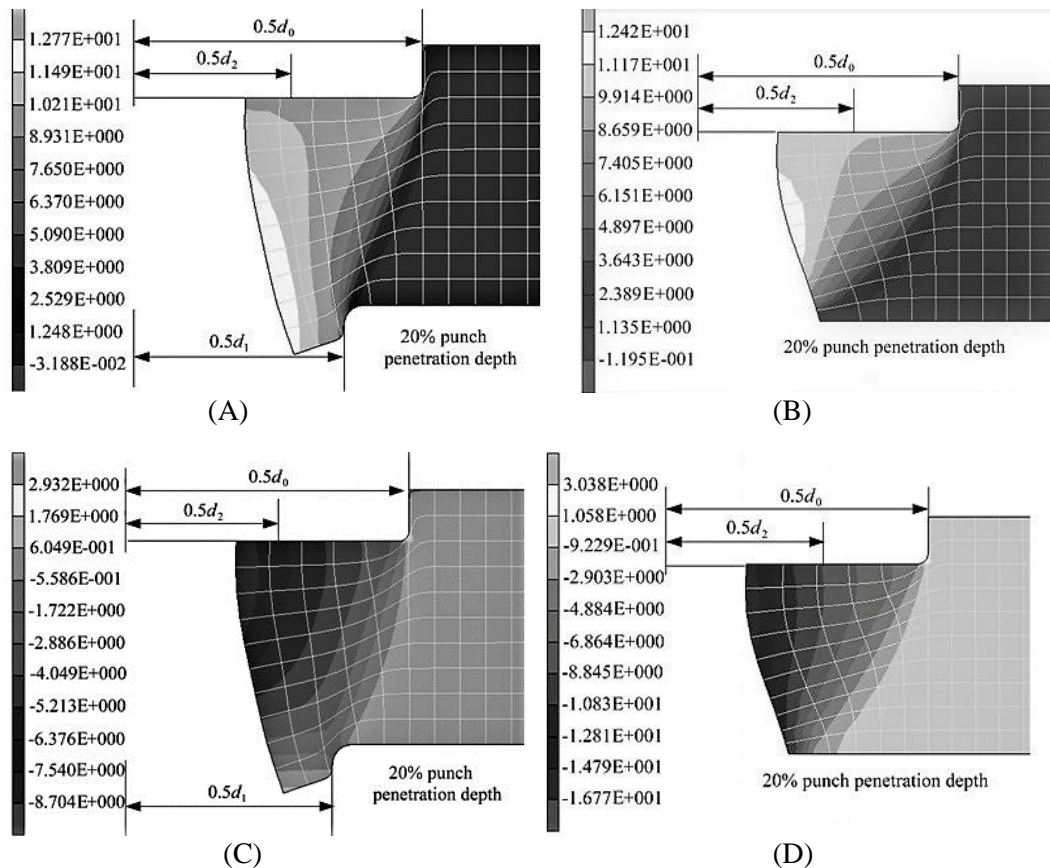


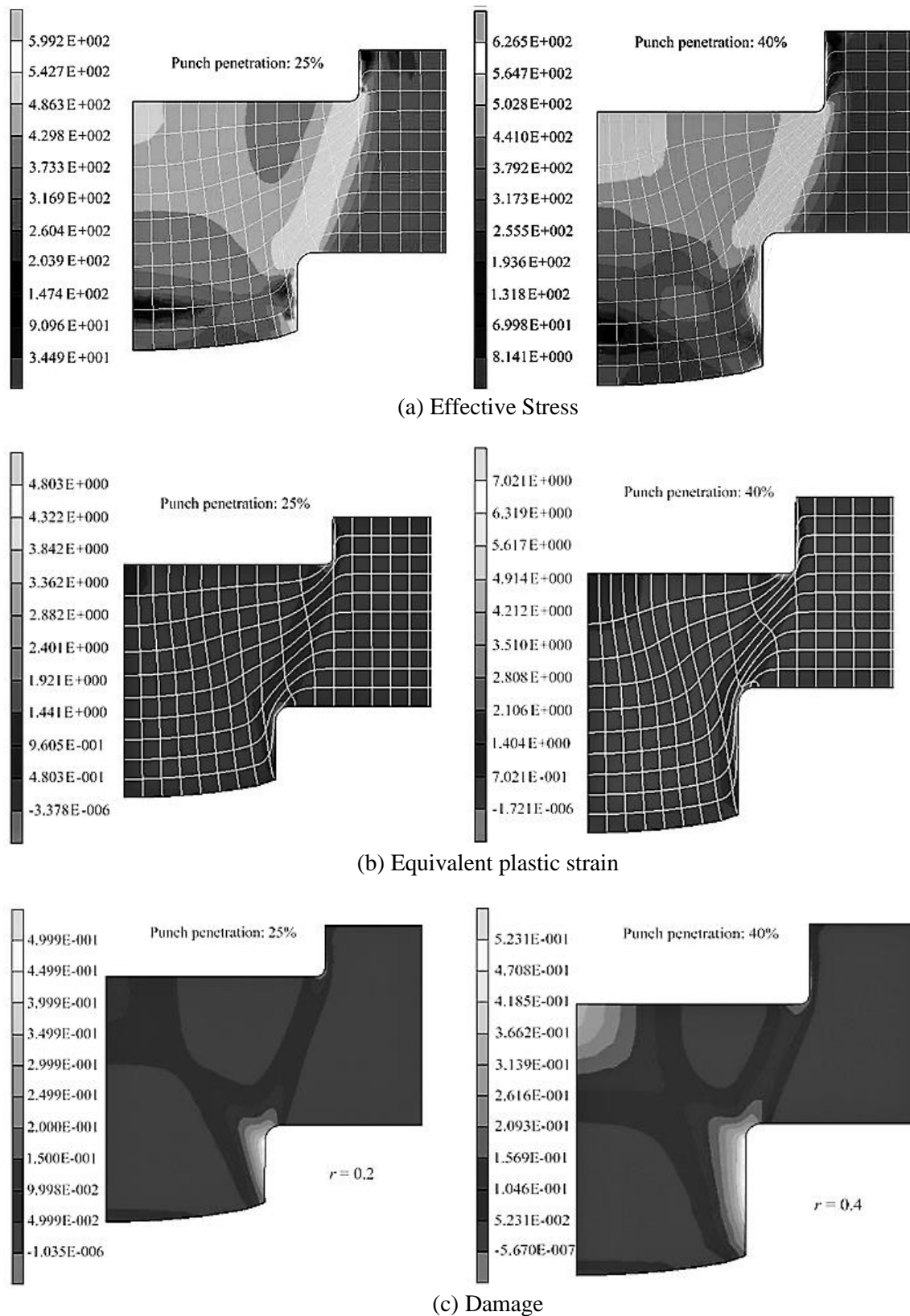
**Figure 13.** Metal flow under different  $d_2$ . (a)-(b): Axial velocity; (c)-(d): Radial velocity.

### STRESS AND STRAIN DISTRIBUTIONS

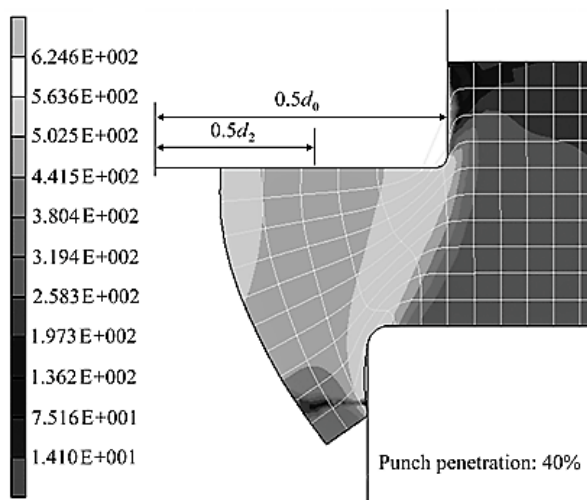
The distribution of effective stress, equivalent plastic strain, and damage is depicted in Figure 14 a, illustrating the effects when the punch penetrates the material thickness by 25% and 40%. Upon examining the distribution of each state variable, it is evident that deformation primarily occurs in the region between the punch and die edge, as well as the area adjacent to the centre of the end surface of the extrusion punch. These areas exhibit higher levels of effective stress compared to other regions, with a maximum effective stress of up to 626 MPa observed when the punch penetration depth increases to 40%. However, in domain 3, the effective stress remains around 245 MPa, below the yield point. Additionally, due to  $R_p < R_d$ , the stress concentration phenomenon is more pronounced in the punch edge area. It is worth noting that for sheet metal extrusion with a pre-punched hole, the distribution of effective stress shown in Figure 15 exhibits slight variations compared to that without a pre-punched hole.

Figure 14 (b) presents the distributions of equivalent plastic strain under varying punch penetration depths. It is observed that significant deformation occurs predominantly near the punch and die edges. As the punch penetration depth increases from 25% to 40%, the maximum equivalent plastic strain changes from 4.8 to 7.02. In the case of sheet metal extrusion with a pre-punched hole, the weaker

constraint on metal flow in the radial direction leads to a slightly smaller maximum equivalent plastic strain of 6.794 than sheet metal extrusion without a pre-punched hole, as shown in Figure 16.



**Figure 14.** Distributions of stress, strain and damage (C15E,  $t = 5$  mm).



**Figure 15:** Distribution of effective stress (C15E,  $t = 5$  mm)

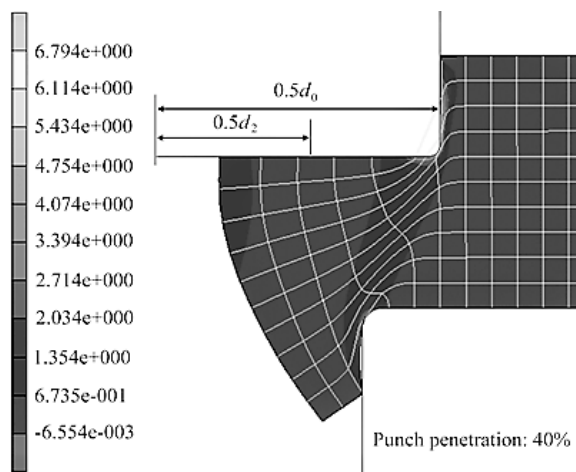


**Figure 16.** Distribution of equivalent plastic strain.

The distribution of ductile damage reveals that significant damage is concentrated in the punch and die edge area, as well as the sidewall of the punch and die extrusion outlet. This damage pattern correlates closely with the equivalent plastic strain experienced in these regions. Notably, the sidewall of the die extrusion outlet exhibits the highest level of damage due to substantial tensile stress and relatively low hydrostatic stress in that specific area.

Moreover, the radius of the die edge plays a pivotal role in influencing the extent of damage. As depicted in Figure 14 (c), a decrease in the radius of the die edge from 0.4 mm to 0.2 mm results in an increase in the maximum damage value under a punch penetration depth of 40%, rising from 0.52 to 0.68. This implies that a smaller die edge radius leads to more extensive damage, while the location of the maximum damage remains unchanged. Consequently, selecting an appropriate radius for the die edge becomes crucial in minimizing the occurrence of defective products.

### INFLUENCE OF PRE-PUNCHED HOLE ON THE FORCE

Figure 17 presents the force-stroke curves obtained from combinations of  $d_0$ ,  $d_1$ , and  $d_2$ . Analyzing these curves allows us to gain insights into the forming mechanism.

By comparing curves 1, 5, and 7, where  $d_2=0$ , it becomes evident that a smaller  $d_0/d_1$  ratio results in a larger forming force. This observation holds true even when  $d_2$  is equal to zero. Similar trends can be observed in curves 2 and 8, as well as curves 3 and 9.

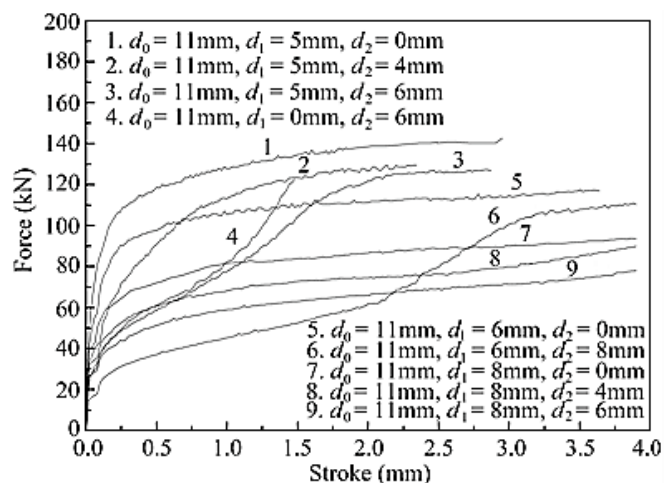


**Figure 17.** Force-stroke curves under different  $d_0$ ,  $d_1$ , and  $d_2$ .

An analysis of curves 1, 2, and 3 reveals that the presence of a pre-punched hole reduces the overall forming force. Including a pre-punched hole divides the deformation process into two stages: "ring upsetting" and "extrusion." The dominant process varies depending on the combination of pre-punched holes and extrusion outlets.

When the diameter of the pre-punched hole is larger than that of the extrusion outlet, the "ring upsetting" process lasts longer, causing the transition to the "extrusion" process to occur later. This is evident in curves 2 and 3. In the initial stages, the forming force is lower compared to other situations. As the punch penetration depth increases, the axial restriction weakens. Consequently, the forming force-stroke curve resembles curve 2, which corresponds to the situation where  $d_2 < d_1$ .

## CONCLUSIONS

This paper focuses on simulating the sheet metal extrusion process with various combinations of  $d_0$ ,  $d_1$ , and  $d_2$  using an ALE-FEM approach. Through the analysis conducted, several key characteristics regarding the metal flow behavior and forming force have been summarized as follows:

- The deformation zone of the sheet metal extrusion process can be divided into three distinct domains, namely deformed, deforming, and rigid, based on the combination of axial and radial velocities.
- A shrinkage cavity is an incidental phenomenon that occurs during sheet metal extrusion due to extrusion and penetration. However, increasing  $R_d$  helps restrain the occurrence of shrinkage cavities, while the effect is terminated with the rise of  $R_p$ .
- Damage is primarily concentrated in the punch and die edge area and the sidewall of the punch and die extrusion outlet, with the maximum damage typically observed on the sidewall of the die extrusion outlet. A smaller  $R_d$  leads to more significant damage without altering its location. Thus, implementing an appropriate radius for the die edge can effectively reduce the likelihood of producing poor-quality products.
- The presence of a pre-punched hole results in a decrease in the total forming force. A smaller  $d_0/d_1$  ratio also corresponds to a larger forming force. The predominant process, such as "ring upsetting" or "extrusion," varies depending on different combinations of  $d_1$  and  $d_2$ . As the punch penetration depth increases, the predominant process transforms, and this trend is observed from the force-stroke curve.

In conclusion, this study provides valuable insights into the sheet metal extrusion process, shedding light on metal flow behavior, shrinkage cavity formation, damage distribution, and the influence of pre-punched holes on forming forces.

## REFERENCES

1. RA Schmidt, F Birzer, P Hofel, et al. "Cold Forming and Fine blanking." A Handbook on Cold Processing, Steel Material Properties, Part Design, Switzerland, 2007, 65–116.
2. PF Zheng, LC Chan, TC Lee. "Numerical Analysis of the Sheet Metal Extrusion Process." *Finite Elements in Analysis and Design* 42 (3) (2005): 189–207.
3. ZH Chen, CY Tang, LC Chan, et al. "Simulation of the Sheet Metal Extrusion Process by the Enhanced Assumed Strain Finite Element Method." *Journal of Materials Processing Technology* 91 (1–3) (1999): 250–56.
4. ZH Chen, TC Lee, CY Tang. "Numerical Simulation of a Sheet Metal Extrusion Process by Using Thermal-Mechanical Coupling EAS FEM." *Journal of University of Science and Technology Beijing* 9 (5) (2002): 378–82.
5. XC Zhuang, Z Zhao, H Xiang. "Simulation of Sheet Metal Extrusion Processes with Arbitrary Lagrangian-Eulerian Method." *Transactions of Nonferrous Metals Society of China* 18 (5) (2008): 1172–76.
6. HY Li, XC Zhuang, Z Zhao. "Research on Material Flow Stress Models in Common Use." *Die and Mould Technology* 5 (2009): 1–4.
7. P Hora. "Advanced Constitutive Models as Precondition for an Accurate FEM-Simulation in Forming Applications." In *Proceedings of the 5th German LS-DYNA Forum*, Ulm, German, 2006.
8. PJ McAllen, P Phelan. "Comparison of Ductile Failure Models Using a Simple Elastic-Plastic Based Degradation Model." *Journal of Materials Processing Technology* 155–156 (2004): 1214–19.
9. JR Rice, DM Tracey. "On the Ductile Enlargement of Voids on Tri-axial Stress Fields." *Journal of Mechanics and Physics of Solids* 17 (3) (1969): 201–17.
10. Z Zhao, XC Zhuang, XL Xie. "An Improved Ductile Fracture Criterion for Fine-Blanking Process." *Journal of Shanghai Jiaotong University (Science)* 13(6) (2008): 702–6.
11. F Cen, T Xing, K T Wu. "Real-Time Performance Evaluation of Line Topology Switched Ethernet." *International Journal of Automation and Computing* 5(4) (2008): 376–80.
12. ZP Lin, SS Xie, J Chen. "Experimental Method for Metal Plastic Forming." Beijing, PRC: Metallurgy Industry Press, 2002, 33–40.